A&A 474, 1061–1071 (2007)
DOI: 10.1051/0004-6361:20078210

Astronomy & Astrophysics

H-atom bombardment of CO_2, HCOOH, and CH_3CHO containing ices

S. E. Bisschop, G. W. Fuchs, E. F. van Dishoeck, and H. Linnartz

Raymond and Beverly Sackler Laboratory for Astrophysics, Leiden Observatory, Leiden University, PO Box 9513, 2300 RA Leiden, The Netherlands
e-mail: bisschop@strw.leidenuniv.nl

Received 3 July 2007 / Accepted 11 September 2007

ABSTRACT

Context. Hydrogenation reactions are expected to be among the most important surface reactions on interstellar ices. However, solid state astrochemical laboratory data on reactions of H-atoms with common interstellar ice constituents are largely lacking.
Aims. The goal of our laboratory work is to determine whether and how carbon dioxide (CO_2), formic acid (HCOOH) and acetaldehyde (CH_3CHO) react with H-atoms in the solid state at low temperatures and to derive reaction rates and production yields.
Methods. Pure CO_2, HCOOH and CH_3CHO interstellar ice analogues are bombarded by H-atoms in an ultra-high vacuum experiment. The experimental conditions are varied systematically. The ices are monitored by reflection absorption infrared spectroscopy and the reaction products are detected in the gas phase through temperature programmed desorption. These techniques are used to determine the resulting destruction and formation yields as well as the corresponding reaction rates.
Results. Within the sensitivity of our set-up we conclude that H-atom bombardment of pure CO_2 and HCOOH ice does not result in detectable reaction products. The upper limits on the reaction rates are $\leq 7 \times 10^{-17}$ cm^2 s^{-1} which make it unlikely that these species play a major role in the formation of more complex organics in interstellar ices due to reactions with H-atoms. In contrast, CH_3CHO does react with H-atoms. At most 20% is hydrogenated to ethanol (C_2H_5OH) and a second reaction route leads to the break-up of the C–C bond to form solid state CH_4 (~20%) as well as H_2CO and CH_3OH (15–50%). The methane production yield is expected to be equal to the summed yield of H_2CO and CH_3OH and therefore CH_4 most likely evaporates partly after formation due to the high exothermicity of the reaction. The reaction rates for CH_3CHO destruction depend on ice temperature and not on ice thickness. The results are discussed in an astrophysical context.

Key words. astrochemistry – molecular data – ISM: molecules – methods: laboratory – molecular processes

1. Introduction

It is generally assumed that at the low temperatures in interstellar clouds, thermal hydrogenation of molecules on icy grain surfaces is the main mechanism to form more complex saturated species (Tielens & Charnley 1997). This is due to the relatively high abundance of H-atoms in the interstellar medium as well as their high mobility even on cold grains. However, most of the reactions in the proposed reaction schemes have not yet been measured experimentally. Hiraoka et al. (1994, 2002), Watanabe et al. (2004), Hidaka et al. (2004) and Fuchs et al. (2007) have studied reactions of thermal H-atoms with CO ice in the laboratory, and shown that H_2CO, and at higher fluxes also CH_3OH, are readily formed at temperatures as low as 12 K. It thus seems likely that other species will also be able to react with H-atoms to form saturated grain-surface products. These species may be the starting point for an even more complex chemistry that occurs at higher temperatures or by energetic processing due to UV or cosmic rays in the ice. Eventually, the ices will evaporate when heated by a protostar, leading to the complex organics seen in hot cores (e.g., Blake et al. 1987; Ikeda et al. 2001). The aim of this paper is to study the reactivity of a number of astrophysically relevant molecules with H-atoms in interstellar ice analogues at low temperatures to test the proposed thermal hydrogenation reaction scheme and to characterize which products are formed and which mechanism is involved.

Interstellar ices contain both simple and complex species (see Ehrenfreund et al. 1999). The most abundant ice molecules are H_2O, CO and CO_2, which have very strong vibrational modes. The spectroscopic identification of other less abundant ices, such as HCOOH and CH_3CHO studied here, relies on weaker bands i.e., the OH and CH bending modes, ν_B(OH/CH), of HCOOH at 7.25 μm and the CH_3 deformation, $\nu_D(CH_3)$, of CH_3CHO at 7.41 μm. Solid state abundances of HCOOH are 1–5% in both low and high mass star forming regions with respect to H_2O (Schutte et al. 1997, 1999; Gibb et al. 2004; Boogert et al. 2004). The detection of CH_3CHO is less certain, but abundances up to 10% have been reported (Gibb et al. 2004; Keane et al. 2001).

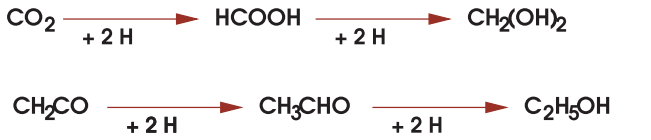

Fig. 1. Potential reaction routes for hydrogenation of CO_2 and CH_2CO ice. Only stable products are shown.

The specific species studied in this paper are CO_2, HCOOH and CH_3CHO, molecules that take a central place in inter- and circumstellar hydrogenation reaction schemes (Fig. 1). CO_2, HCOOH and $CH_2(OH)_2$ differ only in their number of hydrogen atoms. It is therefore possible that they are related through successive hydrogenation reactions. Previous laboratory experiments of H_2 and CO_2 have resulted in the formation of HCOOH on ruthenium surfaces (Ogo et al. 2006), but this reaction may have been mediated by the catalytic surface.

Another series of organics that are thought to be linked through successive hydrogenation are CH_2CO, CH_3CHO and C_2H_5OH (Fig. 1). Ethanol is indeed detected in warm gas phase environments in star-forming regions but CH_2CO and CH_3CHO are found mostly in colder gas (Ikeda et al. 2001; Bisschop et al. 2007b). This may be either due to very efficient conversion of CH_3CHO into C_2H_5OH or because the latter species may be formed through another route. In particular, astronomical observations show a constant CH_3OH/C_2H_5OH ratio which indicates that these two species are chemically linked (Bisschop et al. 2007b).

H-addition reactions in astrophysically relevant ices have been studied previously through UV photolysis experiments, where the hydrogen atoms are produced by dissociation of a suitable precursor molecule, often H_2O ice (e.g., Ewing et al. 1960; Milligan & Jacox 1964, 1971; Van Ijzendoorn et al. 1983; Allamandola et al. 1988; Gerakines et al. 2000; Moore et al. 2001; Wu et al. 2002). Although these experiments give a useful indication whether certain hydrogenation reactions may or may not occur, their results cannot be compared directly with those obtained from the laboratory studies mentioned above, nor can they be used to quantitatively test reaction schemes such as those in Fig. 1 (see Sect. 2.2 for details).

This paper is organized as follows: Sect. 2 explains the experimental method, Sect. 3 focuses on the data reduction and analysis, Sects. 4–6 discuss the results, derived reaction rates and chemical physical mechanisms for hydrogenation reactions with HCOOH, CO_2 and CH_3CHO, Sect. 7 presents the astrophysical implications and finally Sect. 8 summarizes the main conclusions of this study.

2. Experiments

2.1. Our experiment

The experiments are performed using a new ultra-high vacuum set-up that comprises a main chamber and an atomic line unit. The details of the operation and performance of the set-up are described by Fuchs et al. (2007). The main chamber contains a gold coated copper substrate (2.5×2.5 cm^2) that is mounted on top of the cold finger of a He cryostat. Temperatures can be varied between 12 and 300 K with 0.5 K precision using a Lakeshore 340 temperature control unit and are monitored with two thermocouples (0.07% Au in Fe versus chromel) that are mounted on the substrate face and close to the heater element. The typical pressure in the main chamber during operation is better than 5×10^{-10} mbar.

Pure ices of $^{13}C^{18}O_2$ (97% purity, Icon), $^{12}C^{18}O_2$ (97% purity, Icon), HCOOH (98% purity, J. T. Baker) and CH_3CHO (99% purity, Aldrich) as well as mixed ices of $^{13}C^{18}O_2$ with H_2O (deionized) and CO (99.997% purity, Praxair) are studied (see Table 1, for an overview of the mixture ratios, ice thicknesses and ice temperatures). The two isotopologues of CO_2 are used to distinguish between atmospheric CO_2 and solid CO_2 processed by H-atoms. The ices are grown at 45^0 with a flow of 1.0×10^{-7} mbar s^{-1} where 1.3×10^{-6} mbar s^{-1} corresponds to 1 monolayer (ML) s^{-1}. The temperatures of the ices range from 12 to 20 K and their thicknesses are chosen between 8 and 60 ML.

H-atoms are produced in a well-studied thermal-cracking device (Tschersich & von Bonin 1998; Tschersich 2000). The dissociation rate and resulting H-atom flux depend on the temperature and pressure which are both kept constant during a single experiment. The temperature of the heated tungsten filament, T_W is ~2300 K in all experiments and the H+H_2 flow through the capillary in the atom line is either 1.0×10^{-4} or 1.0×10^{-5} mbar s^{-1}. For the latter pressure the calculated dissociation rate, α_{dis}, in the atomic line is 0.45. The atoms that exit the source are hot. Before the H-atoms enter the main chamber, they pass through a quartz pipe and equilibrate to ~300 K. The minimum number of collisions of H-atoms with the quartz pipe is 4 due to the nose-shaped form of the pipe. Since H-atoms are thermalized with the surface after only 2–3 collisions, it is expected that most H-atoms will have temperatures equal to the quartz pipe of 300 K. Due to collisions with the walls of the pipe and with each other, a fraction of the atoms recombines to H_2. The effective dissociation fraction, α_{dis}^{eff}, and H-atom flux on the sample surface are therefore calculated to be lower than given by Tschersich (2000), i.e., 0.13 and 5.0×10^{14} cm^{-2} s^{-1}, or 0.20 and 7.8×10^{13} cm^{-2} s^{-1} for the chosen flow-rates of 1.0×10^{-4}

Table 1. Summary of all H-atom bombardment experiments for pure CO_2, HCOOH and CH_3CHO ices, as well as the mixed morphologies. The total time that the ices are exposed to H-atoms are indicated with t and the temperature of the tungsten filament with T_W. A value T_W of 2300 K refers to an experiment in which H_2 is dissociated and of 600 K to control experiments of ices bombarded with H_2-molecules.

Thickness (ML)	T_{ice} (K)	t (min)	T_W (K)	H-fluence (molecules cm^{-2})
CO_2				
15	12.5	180	2300	5.4(18)
15	14.5	180	2300	5.4(18)
15	14.5	180	600	–
CO_2:H_2O				
15[a]	14.5	180	2300	5.4(18)
15[b]	14.5	180	2300	5.4(18)
15[c]	14.5	180	2300	5.4(18)
15[a]	14.5	120	2300	3.6(18)
15[a]	14.5	180	600	–
CO:$^{13}C^{18}O_2$				
30[d]	14.6	180	2300	5.4(18)
15[d]	14.6	180	2300	5.4(18)
30[d]	14.6	180	2300	5.4(18)
45[d]	14.6	180	2300	5.4(18)
15[e]	14.6	180	2300	5.4(18)
30[e]	14.6	180	2300	5.4(18)
HCOOH				
20	12.5	240	2300	7.2(18)
20	40.0	240	2300	7.2(18)
20	12.5	240	600	—
HCOOH:H_2O[f]				
40	12.5	180	2300	5.4(18)
CH_3CHO				
16.2	14.5	180	2300	5.4(18)
7.8	14.5	180	2300	5.4(18)
11.4	14.5	180	2300	5.4(18)
13.5	14.5	180	2300	5.4(18)
18.8	14.5	180	2300	5.4(18)
21.2	14.5	180	2300	5.4(18)
22.1	14.5	180	2300	5.4(18)
56.0	14.5	180	2300	5.4(18)
45.8	14.5	180	2300	5.4(18)
11.4	12.4	180	2300	5.4(18)
11.3	17.4	180	2300	5.4(18)
11.2	19.3	180	2300	5.4(18)
11.7	14.5	180	600	—

[a] 39:61% $^{13}C^{18}O_2$:H_2O, [b] 22:78% $^{13}C^{18}O_2$:H_2O, [c] 48:52% $^{13}C^{18}O_2$:H_2O, [d] 45:55% $^{13}C^{18}O_2$:CO, [e] 80:20% $^{13}C^{18}O_2$:CO, [f] HCOOH:H_2O 20:80%.

and 1.0×10^{-5} mbar s^{-1}, respectively (Fuchs et al. 2007). Note also that, the absolute number of H-atoms on the surface at a given time is not equal to the surface flux, because processes such as scattering and recombination take place on the surface. Theoretical simulations show that a steady-state H-atom coverage of 5.0×10^{14} cm^{-2} s^{-1} with an error of a factor 2 is quickly reached in this regime independent of the exact H-atom flux (Cuppen, private communication). A more extensive discussion of the derivation of these steady-state numbers is given by Fuchs et al. (2007). The time and H-fluence, i.e., the total number of atoms cm^{-2} integrated over time in each experiment are listed in Table 1. At the temperatures and fluxes used in our experiment, the substrate surface will be covered with H_2 in a few seconds. Since H_2 molecules do not stick to other H_2 molecules, the maximum coverage with H_2 will only be a few monolayers. H-atoms therefore have to diffuse through the cold H_2 layer before reaching the ice and will be completely thermalized with the surface at the moment they encounter the ice sample. Experiments with only H_2 molecules have been performed for comparison by setting the source temperature T_W to ~600 K as an additional check to confirm that reactions are due to H-atoms and not to H_2 molecules (see Table 1).

The ices are monitored by Reflection Absorption Infrared Spectroscopy (RAIRS) using a Fourier Transform Infrared Spectrometer, covering 4000–700 cm^{-1} with a spectral resolution of 4 cm^{-1}. The infrared path length is the same for all experiments. Typically 512 scans are co-added. An experiment starts with a background RAIR scan and subsequently an ice is deposited onto the substrate surface. Another RAIR spectrum is taken after deposition to determine the initial number of molecules in the ice. An additional background spectrum is recorded afterward such that subsequently recorded spectra yield difference spectra between ices before and after H-atom bombardment. The next step in the experiments is the continuous H-atom bombardment of the ice during which a RAIR scan is taken every 10 min. After 3 h the experiment is stopped and a Temperature Programmed Desorption (TPD) spectrum is obtained using a quadrupole mass spectrometer. The ramp speed is 2 K min^{-1} and is continued until the temperature reaches 200 K. Control experiments with pure ices of CO_2, C_2H_5OH, CH_4 and CH_3OH are studied to determine RAIR band strengths and to calibrate the production yields that are measured using the mass spectrometer (see Sect. 3.3). In those cases RAIR spectra are taken right after deposition and subsequently TPD spectra are recorded as described here for the other experiments.

2.2. Comparison with other hydrogenation experiments

A large number of photolysis experiments of astrophysically relevant ices exist where H-atoms are produced through photo dissociation of H_2O or other precursors (e.g., Ewing et al. 1960; Milligan & Jacox 1964, 1971; Van Ijzendoorn et al. 1983; Allamandola et al. 1988; Gerakines et al. 2000; Moore et al. 2001; Wu et al. 2002). These give useful information on potential hydrogenation reactions schemes, but do not give specific information about reaction rates (see for example Sects. 4.3 and 6.3). Also the question whether thermal hydrogenation reactions can be responsible for newly formed species is not answered, for several reasons. First, the hydrogen atoms resulting from photolysis are produced in situ inside the ice with an excess energy of several eV; such atoms can travel significant distances through the ice (e.g., Andersson et al. 2006) and a reaction may take place before thermalization is achieved. Thus, activation energy barriers can be overcome, in contrast to thermal hydrogenation reactions where this is less probable. Second, although dilution in an inert Ar matrix can stabilize the H-atoms, the H-atom flux on the reactants remains poorly characterized. Third, other reactive products such as OH are also formed by photolysis of H_2O which makes it hard to discriminate the different effects. It is not possible to study pure ices through this method since H_2O or another precursor is always needed to provide a source of H-atoms. Finally, the photolysis experiments reported so far have been carried out under high vacuum conditions (typically 10^{-7} mbar) in which several monolayers of background gases (mostly H_2O) are accreted in less than a minute, providing additional molecules that can be photolyzed during the experiments. This may affect the outcome. In contrast, our experiments and the previously mentioned surface science experiments on CO hydrogenation are performed under ultra-high vacuum conditions (typically 10^{-10} mbar) in which less than a monolayer of background gas (mostly H_2) is accreted during the time-scale of the experiments (a few hours). Here the H-atoms are formed by a microwave source or by thermal cracking and are thermalized to room temperature or less before striking the ice surface, rather than being produced inside the ice.

Table 2. Overview of the integrated frequency ranges with corresponding spectral assignment and band strength. The error on S_X^{ref} amounts to ~30–40%.

Species	Mode	Integration range (cm^{-1})	S_X^{ref} (cm $molecule^{-1}$)
$^{13}C^{18}O_2$[a]	ν_3	2265–2245	1.3(−17)
$^{13}C^{18}O_2$[b]		2265–2245	8.8(−17)
$^{13}C^{18}O_2$[c]		2265–2245	4.8(−17)
$^{13}C^{18}O_2$[d]		2265–2245	4.3(−17)
$^{13}C^{18}O_2$[e]		2265–2245	3.2(−17)
$^{13}C^{18}O_2$[f]		2265–2245	2.7(−17)
CO[e]	ν_1	2160–2120	9.5(−18)
CO[f]		2160-2120	6.4(−18)
HCOOH	ν_3	1800–1550	1.3(−16)
CH_3CHO	ν_7	1745–1719	8.0(−18)
CH_3CHO		1365–1330	2.8(−18)
CH_3OH	ν_8	1060–990	1.1(−17)
CH_4	ν_4	1320–1290	8.2(−18)

[a] Pure $^{13}C^{18}O_2$, [b] 22:78% $^{13}C^{18}O_2$:H_2O, [c] 39:61% $^{13}C^{18}O_2$:H_2O, [d] 48:52% $^{13}C^{18}O_2$:H_2O, [e] 45:55% $^{13}C^{18}O_2$:CO, [f] 80:20% $^{13}C^{18}O_2$:CO.

3. Data analysis

3.1. RAIR analysis

Different frequency ranges are selected for baseline subtraction that depend on the species under study. Fourth order polynomial baselines are fitted to the recorded RAIR spectrum. Additionally, local third order polynomial baselines are subtracted around the features of interest to accurately determine the integrated absorption. The frequency ranges are given per ice morphology in Table 2. From the integrated intensity of the infrared bands, the column density of species X in the ice is calculated through a modified Lambert-Beer equation:

$$N_X = \frac{\ln 10 \int A \, d\nu}{S_X^{ref}}, \quad (1)$$

where the ln10 is needed to convert the integrated absorbance, A, to optical depth and S_X^{ref} is the experimental RAIR band strength of species X. Transmission band strengths available from the literature cannot be used, because the total number of molecules probed with RAIRS cannot directly be related to a value probed in a transmission absorption experiment. This is because the incident beam goes through the ice layer twice with an angle to the surface. Instead, values of S_X^{ref} have been calculated from a calibration experiment without hydrogenation where the deposition rate is 1.0×10^{-7} mbar s^{-1} to grow a layer of typically 10 to 20 ML and where the sticking probability is assumed to be 1. It should be noted that these experimental values can differ between different experimental set-ups and even for the same set-up over time, because they are determined by intrinsic properties such as the alignment of the system. They should therefore not be used to compare directly with observations of interstellar ices and even a comparison between different experiments should be made with caution. The values for S_X^{ref} as well as the spectral assignments of the vibrational modes are summarized for all species in Table 2.

There are several contributions to the uncertainty in the experimentally measured band strengths. The largest fraction comes from the actual deposition and sticking onto the surface. Since our experiment does not contain a micro-balance, the absolute number of molecules on the surface is not known and the possibility that some molecules freeze out on other surfaces than the Au substrate cannot be ruled out. This leads to systematic errors for S_X^{ref} but there is no effect on the relative error for S_X^{ref} between different experiments with the same ice morphology. Based on experiments aimed at the same ice thickness, inaccuracies in the deposition flow are estimated to be ~30%. Since the integrated area of the absorption band is determined very precisely for the deposited species, the column densities can be accurately normalized, but the derived band strengths cannot. Another source of uncertainty for ice mixtures is the precision of the mixing ratio, which is of the order of 10% (see also Öberg et al. 2007; Bisschop et al. 2007a). In summary, the actual uncertainty on the band strengths is substantial and ranges from 30–40%, but the relative uncertainty for ices with the same morphology is less than 5%.

3.2. Reaction rate calculations

The method for calculating reaction rates is described in detail by Fuchs et al. (2007). In short, a species X can react with H-atoms to form species Z through: $X + H \xrightarrow{k_0} Z$. The column density of X that has reacted, $N_X(t)$, is given by:

$$\frac{dN_X(t)}{dt} = -k_0 N_H N_X, \quad (2)$$

where k_0 stands for the reaction constant and N_H for the surface density of H-atoms. In our experiment the H-atom flux is kept constant and corresponds to 7.8×10^{13} or 5.0×10^{14} cm^{-2} s^{-1}. Furthermore, the atoms have a certain penetration depth as observed in experiments of H-atom reactions with CO (Watanabe et al. 2004; Fuchs et al. 2007) which means that not all of the deposited parent species are available for the reaction. Consequently, $N_X(t)$ is calculated via:

$$N_X(t) = N_X(0)\ \alpha_0\ (1 - e^{-\beta_0 t}), \quad (3)$$

where α_0 is the fraction of $N_X(0)$ that is available to react and β_0 (in min^{-1}) corresponds to $k_0 N_H/60$ (the factor 60 comes from the conversion of seconds to minutes). In specific cases only upper limits on reaction rates are calculated and then it is assumed that α_0 only includes the uppermost ice layer. Limits based on the column density decrease after 1 min give the most conservative upper limit on β_0. Similar to the cases described by Fuchs et al. (2007), fits to the reaction rate differ when they are made over the complete time-period of the experiment (hrs) or only over a shorter period (minutes).

3.3. TPD analysis and calculation of the production yield

The TPD data provide complementary information on the reaction yields and are important, in particular, for those molecules that are not accurately determined by RAIRS. The TPD data are fitted by second order polynomial baselines. The temperature range over which a baseline is fitted depends on the desorption temperature of a specific species. Calibration experiments of pure ices with a known number of molecules have been performed by measuring the corresponding integrated area of the mass spectrometer signal. The number of molecules N_Z in other experiments has been determined by comparison of the integrated signal to the number of molecules in the calibration experiments. Since pure ices are needed for the calibration, no accurate yields can be calculated for H_2CO which is not readily available as a pure ice due to polymerization (see Sect. 6.1). The yield, Y_Z, of the newly formed species Z in % can then be calculated through:

$$Y_Z = \frac{N_Z}{\alpha_0\ N_X(0)}, \quad (4)$$

where N_Z is the column density as derived from the TPD data, α_0 is taken from the fit of the RAIRS data and $N_X(0)$ is the initial column density of the precursor species as derived from the RAIR spectra.

4. CO_2 containing ices

4.1. Results

Pure ices of CO_2 are bombarded with H-atoms to search for the possible formation of HCOOH following the reaction route as shown in Fig. 1. The reactivity of CO_2 can be tested by recording a decrease in the CO_2 RAIR signal and by monitoring any reaction products. Unfortunately, the CO_2 2300 cm^{-1} ice band is difficult to quantify, because this band overlaps with rotation-vibration transitions of CO_2 present in the purge gas in our spectrometer. The use of $^{13}C^{18}O_2$ isotopic species does not improve this situation. Therefore we have focused on the strongest HCOOH band, the C=O stretching mode, at 1710 cm^{-1}, to monitor formic acid formation. The observed difference RAIR spectrum of $^{13}C^{18}O_2$ bombarded by H-atoms has been compared to that of $^{12}C^{18}O_2$ in Fig. 2a. Both spectra show very weak features at 1730 cm^{-1} and 1500 cm^{-1}, but none at positions typical for HCOOH. The detected bands, however, occur at exactly the same positions as previously seen for H_2CO when formed upon CO hydrogenation (e.g., Watanabe et al. 2004). Furthermore, the features do not shift when a different isotopic species is used, which is expected when the formation involves CO_2 ice. In the TPD spectra of CO_2 ices bombarded with H-atoms for 3 hrs (not shown) mass 29 and 30 amu desorb in two steps around 100 K and 140 K, and the formation of other species is not detected through TPD. These temperatures and masses are identical to what was observed by Fuchs et al. (2007) for H_2CO desorption from CO ices bombarded by H-atoms. During H-atom bombardment an increase in the mass 28 amu signal is observed, which

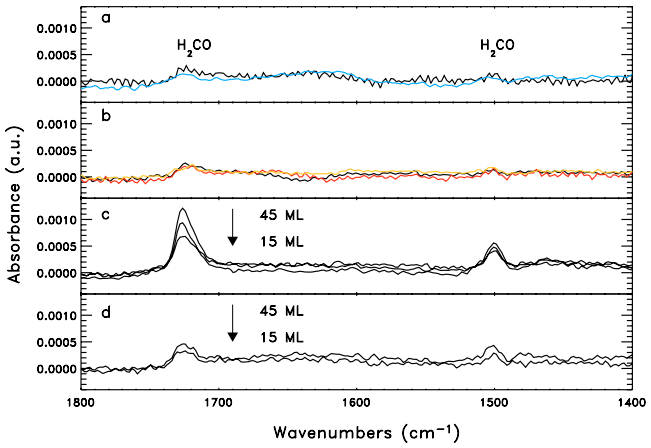

Fig. 2. Difference spectra of the 1800–1400 cm^{-1} range after 180 min of H-atom bombardment. **a)** 15 ML pure $C^{18}O_2$ ice (black line) and $^{13}C^{18}O_2$ (grey line), **b)** 15 ML CO_2:H_2O 39:61% (black line), 22:78% (grey line) and 48:52% (light grey), **c)** 45:55% CO_2:CO mixtures for 15, 30 and 45 ML ice thickness and **d)** 80:20% CO_2:CO mixture for 15 and 30 ML. The temperature of the ice is ~14.5 K. The arrows indicate how the absorbance of the H_2CO bands decreases with decreasing thickness.

is likely due to degassing of both CO and N_2 from the metal parts of our experiment. It is therefore plausible that the measured low level of H_2CO formation observed in the experiment originates from hydrogenation of background gaseous CO and is not related to the CO_2 ice.

To test whether the presence of H_2O affects the reactivity of CO_2 ice upon H-atom bombardment as has been observed for CO in CO:H_2O mixtures (Watanabe et al. 2004; Fuchs et al. 2007), mixtures of 22:78% to 48:52% CO_2:H_2O have been investigated (see Fig. 2b). Like in the experiments with pure CO_2, weak RAIR features of similar intensity are observed at 1730 and 1500 cm^{-1}. Again we assign these features to the C=O stretching mode and the C-H bending mode of H_2CO. Thus, as for the pure ices, a small amount of background CO accretes and forms H_2CO. Within the sensitivity of our experiment, we conclude that CO_2 does not react with H-atoms even if mixed with H_2O.

Finally, mixtures of $^{12}C^{16}O$ and $^{13}C^{18}O_2$ are studied to determine which species is more likely to react upon H-atom bombardment: CO or CO_2. Since CO hydrogenation reactions were previously reported in the literature (Watanabe et al. 2004; Fuchs et al. 2007), the answer to this question must be CO. In Fig. 2c and d, the resulting difference spectra for CO_2:CO mixtures are shown for different ice thicknesses and with mixture concentrations of 45:55% CO_2:CO and 80:20% CO_2:CO, respectively. Similar to H-atom bombardment of pure CO_2 ices and CO_2:H_2O mixtures, no evidence for HCOOH formation is observed in CO_2:CO mixtures. In contrast, CO does react with H-atoms to form H_2CO and CH_3OH as is evidenced by the presence of strong H_2CO absorption features at 1730 and 1500 cm^{-1} and CH_3OH at 1030 cm^{-1}. This is consistent with H-atom bombardment experiments for pure CO and CO:H_2O mixtures by Watanabe et al. (2004) and Fuchs et al. (2007). The complementary TPD data show the same picture of no HCOOH formation and clear H_2CO and CH_3OH formation from CO. Other products than the precursor and product species H_2CO and CH_3OH are not observed.

Table 3. Upper limits on the reaction/destruction rates for HCOOH and CO_2. The uncertainty on k_0 amounts to a factor 2.

Species	Ice matrix	T_{ice} (K)	k_0 (cm^2 s^{-1})
CO_2	pure	14.5	≤6.2(−17)
CO_2	$^{13}C^{18}O_2$:H_2O 39:61%	14.5	≤6.0(−17)
CO_2[a]	$^{13}C^{18}O_2$:H_2O 39:61%	14.5	≤3.8(−17)
CO_2	$^{13}C^{18}O_2$:H_2O 22:78%	14.5	≤6.7(−17)
CO_2	$^{13}C^{18}O_2$:H_2O 48:52%	14.5	≤3.2(−17)
CO_2	$^{13}C^{18}O_2$:H_2O 39:61%	14.5	≤6.0(−17)
HCOOH	pure	12.5	≤2.3(-17)

[a] Limit derived for experiment without bombardment.

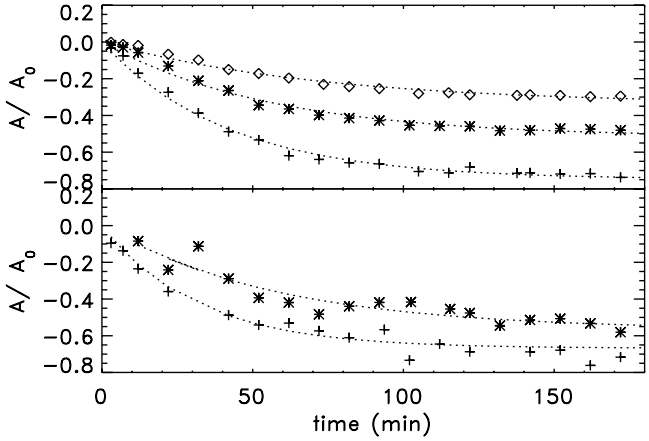

Fig. 3. A/A_0 for the CO 2140 cm^{-1} band in CO_2:CO mixtures at 14.5 K for the 45:55% (*upper panel*) and 80:20% (*lower panel*). The symbols refer to 15 ML +, 30 ML ∗, and 45 L ◇. The dotted lines indicate the fits to the data.

Table 4. Values for α_0, β_0, and the reaction rate k_0 for CO in CO:CO_2 mixtures at ice temperatures of 14.5 K upon H-atom bombardment. The uncertainties for α_0 and β_0 amount to 10–20% and for k_0 are a factor 2.

Ice mixture	Ice thickness CO_2/total (ML)	α_0	β_0 (min^{-1})	k_0 (cm^2 s^{-1})
45:55% CO_2:CO	8/15	0.75	0.024	2.9(−15)
45:55% CO_2:CO	17/30	0.51	0.018	2.2(−15)
45:55% CO_2:CO	25/45	0.34	0.014	1.7(−15)
80:20% CO_2:CO	3/15	0.67	0.032	3.8(−15)
80:20% CO_2:CO	6/30	0.57	0.017	2.0(−15)

4.2. Reaction rates

No hydrogenation products of CO_2, specifically HCOOH, are observed within the experimental sensitivity. The limit on the formation reaction rate for HCOOH from CO_2 is ≤7.0×10^{-17} cm^2 s^{-1} based on the limit on the column density for HCOOH after 1 min of H-atom bombardment for all ice morphologies (see Sect. 3.2 for the derivation and Table 3 for the individual values for each experiment).

In Fig. 3 the absorbance divided by the initial absorbance at $t = 0$, A/A_0, is shown for the 45:55% and 80:20% CO_2:CO ice mixtures. The data are fitted as described in Sect. 3.2 and the fits are indicated in Fig. 3 with dotted lines. The resulting values for α_0 and β_0 as well as the k_0 are given in Table 4. Since

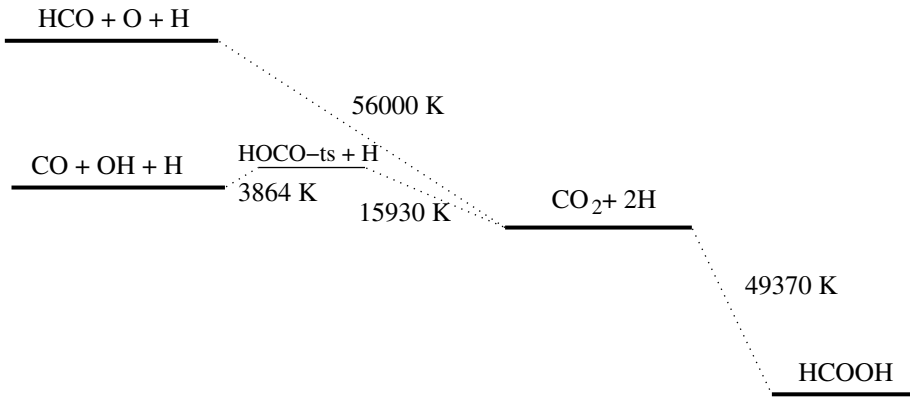

Fig. 4. Potential energy scheme for CO_2 dissociation and hydrogenation. The relative energies are based on the heats of formation at 0 K. The scale in electronvolts is indicated on the right. The heats of formation are derived from Cox et al. (1989) for H, CO_2, CO and O, from Ruscic et al. (2002) for OH, from Gurvich et al. (1989) for HCO and HCOOH and from Lakin et al. (2003) for the HOCO transition state (ts).

the H_2CO band strength could not be determined accurately in these experiments only α_0 and β_0 are fitted. Clearly α_0, i.e., the fraction of CO molecules available for reaction, decreases with increasing ice thickness.

4.3. Discussion and conclusion

Previously, CO_2+H reactions have been studied by Milligan & Jacox (1971) in UV-photolysis experiments of Ar:CO_2:H_2O matrices. Only the formation of more oxygen-rich species such as CO_3 has been observed, but not HCOOH. Although these results cannot be compared directly with ours (see Sect. 2.2), our findings are consistent with theirs that CO_2 does not react readily with H-atoms. To explain the lack of CO_2 hydrogenation reactions, Fig. 4 presents the relative formation energies of possible products. Reaction of CO_2 with H-atoms to either HCO+O or CO+OH is energetically highly unfavorable. This is due to the HOCO transition state being ~15 930 K (1.4 eV) higher in energy compared to CO_2+H in the gas phase (Lakin et al. 2003). On the other hand, a hydrogenation reaction could be expected based on the higher heat of formation of CO_2+2H with respect to HCOOH of ~49 370 K (4.3 eV). Indeed, in the chemical physics literature CO_2 is found to hydrogenate to HCOOH on ruthenium and iridium catalysts through formate complexes with the catalyst (Ogo et al. 2006). The chemically bonded formate species subsequently reacts with H_3O^+ to form HCOOH. This reaction mechanism requires acidic species as well as a catalytic surface that are not present in the current experiment. Hwang & Mebel (2004) calculated a potential energy surface for the gas phase H_2 + CO_2 reaction. The HCOOH end product is higher in energy than the initial species by ~2600 K (0.22 eV), but the CO_2 + 2H reaction is exothermic (see Fig. 4). For the reaction of CO_2 with H-atoms or H_2 the same transition state H_2CO_2, a complex cyclic structure, has to be overcome. This transition state lies 35 000–37 000 K (3.0–3.2 eV) above the starting point, CO_2 + H_2, but below CO_2 + 2 H. This step can therefore not be rate-limiting for the CO_2+ 2H → HCOOH reaction. Since the reaction is clearly not observed in our experiment, the rate determining step must be the addition of the first hydrogen atom to CO_2 to form HCO_2 and the barrier to this reaction must be too high to be overcome for the ice temperatures of 12–60 K as used in our experiments.

Several recent studies have focused on reactions of CO + H leading to the formation of H_2CO and CH_3OH. Fuchs et al. (2007) find that even for the lowest ice thicknesses of 1 to 2 ML 30% of the ice is hidden from the impinging H-atoms. At higher thicknesses α_0 increases and there is a maximum layer thickness of 12 ML of CO ice that can react with H-atoms. The behavior of α_0 for our CO_2:CO mixtures is consistent with this picture, although at maximum 7±3 ML and 8±3 ML of the CO ice reacts for the 45:55% and 80:20% CO_2:CO mixtures, respectively. In other words mixing CO with CO_2 does not cause more CO to be "hidden" from the H-atom exposure.

Our reaction rates, β_0, of e.g., 0.032 min^{-1} in CO:CO_2 80:20% with 15 ML total ice thickness at 14.5 K are similar to those found for pure CO ices by Fuchs et al. (2007) of ~0.030 min^{-1} (~0.023 min^{-1} when converted to our assumption for the initial number molecules) for a similar amount of CO of 11 ML at 15 K. These rates are the same within the 30–40% uncertainty. However, for CO:H_2O 1:5 mixtures Fuchs et al. (2007) find a value of ~0.11 min^{-1} (0.083 min^{-1}) for 12 ML at 15 K indicating that the reaction rates for CO hydrogenation are significantly higher in mixtures with H_2O ice. The similarity between the reaction rate of CO in mixtures with CO_2 and pure CO ices and the difference between those and CO:H_2O ice mixtures can be explained by CO and CO_2 only interacting through weak Van der Waals forces. The electronic structure of the CO molecule will therefore not differ significantly in mixtures with CO_2 from pure CO ices. H_2O on the other hand has a stronger dipole moment of 1.85 D compared to zero and 0.11 D for CO_2 and CO, respectively, and forms hydrogen bonds. Furthermore it is known that CO strongly interacts with and influences the band strengths of H_2O molecule (Bouwman et al. 2007). Thus, the electronic structure of the CO molecule will be perturbed in mixtures with H_2O, strongly affecting the reaction rate of CO with H-atoms. In summary the presence of CO_2 in ice mixtures with CO does not strongly affect the reactivity of CO with H-atoms.

5. HCOOH containing ices

5.1. Results

Figure 5 shows the difference spectrum for ν_S(C=O) at ~1710 cm^{-1} of pure HCOOH ice bombarded with H-atoms as well as control experiments with bombardment of H_2 molecules at 12 K (for an overview of all infrared features of HCOOH see Cyriac & Pradeep 2005). The growth of an infrared feature around ~1050 cm^{-1} indicative for $CH_2(OH)_2$ formation has not been observed (for an overview of the infrared features of $CH_2(OH)_2$ see Lugez et al. 1994). A decrease on the blue side of the ν_S(C=O) mode at 1710 cm^{-1} of HCOOH is seen at 1750 cm^{-1} as well as an increase at 1730 cm^{-1}, which means that the overall HCOOH band profile changes slightly. At 1730 cm^{-1}, the C=O stretch for H_2CO is located, but other features of H_2CO, such as the 1500 cm^{-1} band, are missing. The decrease corresponds to <0.1 ML derived from our calculated RAIR band

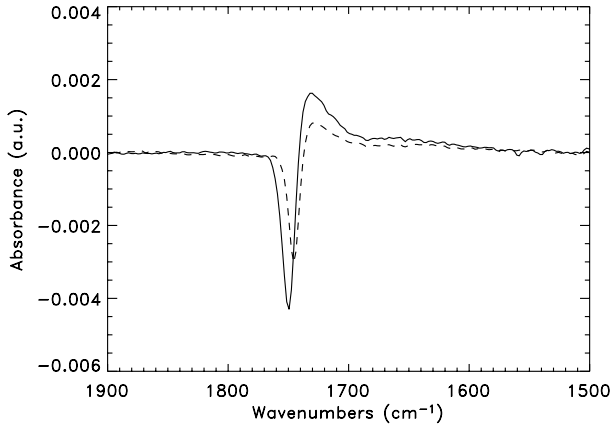

Fig. 5. The difference spectrum of the HCOOH ν_S(C=O) stretch for HCOOH bombarded for 4 hrs with H-atoms at 12 K (solid) and at 40 K (dashed).

strength. These features are present in difference spectra for HCOOH ice bombarded with H-atoms at 12 and 40 K. A similar shift is seen for transmission infrared experiments with pure HCOOH ice that is heated to ∼60 K (Bisschop et al. 2007a). At the same time the ν_S(CH) and ν_S(OH) vibrational modes increase due to conversion of HCOOH in dimeric form to HCOOH organized in chains. In the RAIRS spectra these bands are also seen to increase. Furthermore, the same change in RAIR profile is found for HCOOH ices of 40 K, where H-atoms cannot stick any longer onto the surface, but can only collide. Since the ice has a temperature of 40 K, the reorganization of the ice is less and consequently the signal of the difference spectrum is smaller. In conclusion, the RAIR data do suggest that some restructuring takes place in the surface but no reaction.

With TPD the masses of 48 ($CH_2(OH)_2$), 46 (HCOOH), 45 (HCOO), 44 (CO_2), 32/31 (CH_3OH), 30/29 (H_2CO), and 28 amu (CO) have been monitored during warm-up. No products are detected at 48, 32, 31, or 30 amu to upper limits of <0.01 ML, indicating that HCOOH is neither hydrogenated nor dissociated. Thus, consistent with the lack of a 1500 cm^{-1} H_2CO absorption feature in the RAIRS data, no evidence for H_2CO formation is observed in the TPD experiment. The detected masses 45, 44, and 29 amu are assigned to HCOOH dissociating in the mass spectrometer, because the same relative mass ratios are seen for a TPD spectrum of pure HCOOH ice that is not bombarded by H-atoms. We conclude that within the limits of our experimental set-up the reaction of HCOOH with H-atoms is not efficient at 12 K.

5.2. Reaction rates

Since no unambiguous evidence for HCOOH destruction in the ice is found, it is only possible to derive an upper limit on its reaction rate, presented in Table 3. It is clear that the HCOOH destruction rates are below 2.3×10^{-17} cm^2 s^{-1} as derived from the limit on the column density after 1 min of H-atom bombardment (see Sect. 3.2). As for CO_2 these reaction rates are very low.

5.3. Discussion and conclusion

In chemical physics literature HCOOH hydrogenation on catalytic surfaces has been shown to lead to decomposition of HCOOH rather than methanediol formation (Benitez et al. 1993).

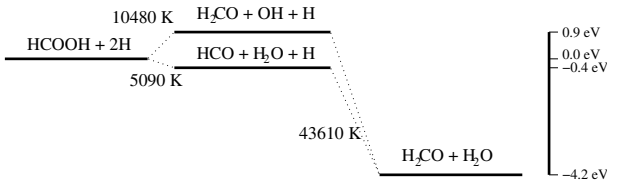

Fig. 6. Potential energy scheme for HCOOH hydrogenation. The energies are based on the heats of formation at 0 K. The energy scale in electronvolts is indicated on the right. The heats of formation are derived from Gurvich et al. (1989) for HCO, H_2CO and HCOOH, from Ruscic et al. (2002) for OH and from Cox et al. (1989) for H and H_2O.

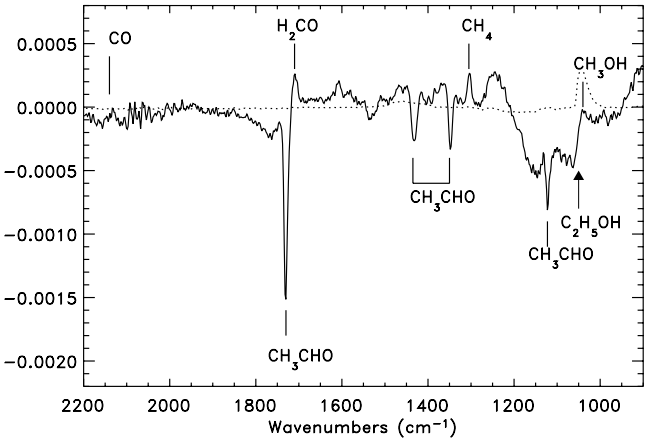

Fig. 7. The difference spectrum of CH_3CHO after 3 h of bombardment with H-atoms. The negative peaks correspond to CH_3CHO destruction, the positive wing around 1700 cm^{-1} is assigned to the ν_S(C=O) mode of H_2CO and the features at 1300 cm^{-1} and 1030 cm^{-1} to $\nu_D(CH_4)$ of CH_4 and ν_S(C–O) of CH_3OH, respectively. The arrow indicates the position where the strongest C_2H_5OH absorption is expected. The dotted line indicates the RAIR spectrum for pure CH_3OH, showing that the feature detected at 1030 cm^{-1} matches that of pure CH_3OH.

HCOOH adsorbs onto such a surface as $HCOO^-$ and H^+ which can be further hydrogenated. The catalytic surface, however, clearly affects the end products and overcomes a reaction barrier that prohibits spontaneous decomposition. If hydrogen atom addition and dissociation occur simultaneously, C–O bond cleavage is more energetically favorable (as shown in Fig. 6). However, it is clear from the results in Sect. 5.1 that no H_2O and H_2CO formation occurs. Thus a high barrier for H-addition to HCOOH must exist for both mechanisms and HCOOH + H reactions in the ice are inefficient.

6. CH_3CHO containing ices

6.1. Results

The infrared spectroscopic features detected for pure CH_3CHO ice match with those detected by Bennett et al. (2005) and Moore & Hudson (1998, 2003). The strongest CH_3CHO band is the C=O stretching mode, ν_S(C=O), at 1728 cm^{-1} (5.79 μm). During H-atom bombardment the intensity decreases, but a small positive wing is observed at 1710 cm^{-1} (see Fig. 7). This band is assigned to the C=O stretching mode of H_2CO. Other CH_3CHO features (e.g., the umbrella deformation mode, ν_D, at 1345 cm^{-1}) also decrease and new bands appear at 1030 and 1300 cm^{-1} that are attributed to the C–O stretching mode of CH_3OH and the deformation mode of CH_4, respectively. No clear absorption is observed at 1050 cm^{-1}, where the strongest

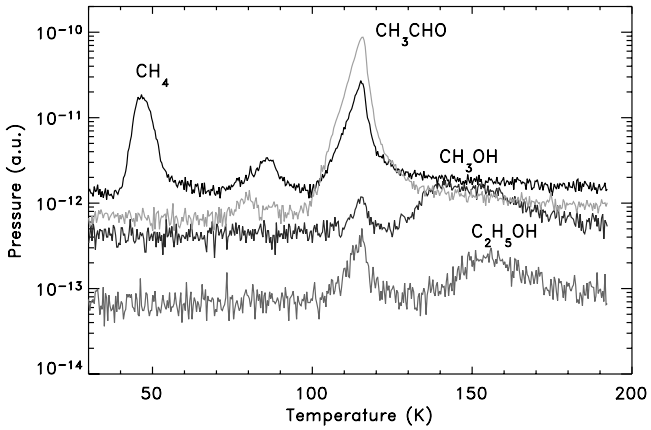

Fig. 8. The TPD spectrum for 40 ML of CH_3CHO bombarded with H-atoms for 3 hrs at 14.5 K. The black line refers to the 16 amu signal (CH_4), dark grey line to 31 amu (CH_3OH), grey to 46 amu (C_2H_5OH) and light grey to 44 amu (CH_3CHO).

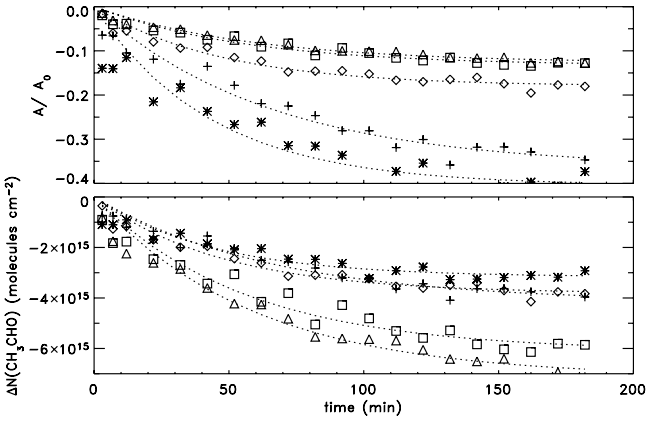

Fig. 9. The A/A_0 ratio (*upper panel*) and $\Delta N(CH_3CHO)$ (*lower panel*) for the CH_3CHO 1345 cm^{-1} band for different ice thicknesses and a constant ice temperature of 14.5 K. The symbols refer to 11.4 ML (+), 7.8 L (∗), 21.2 L (◇), 45.8 ML (□) and 56.0 ML (△). The dotted lines indicate the fits to the data.

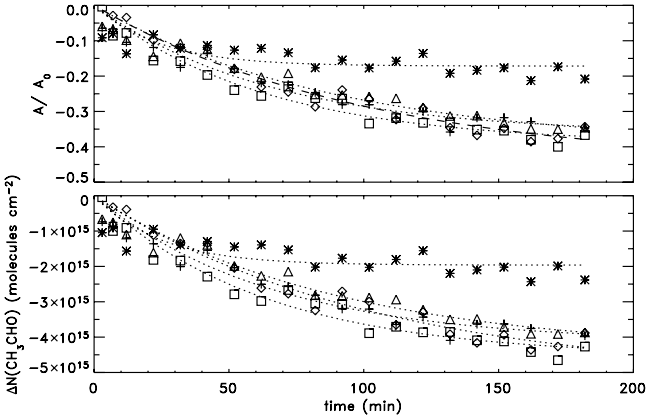

Fig. 10. The A/A_0 ratio (*upper panel*) and $\Delta N(CH_3CHO)$ (*lower panel*) for the CH_3CHO 1345 cm^{-1} band for different ice temperatures and a constant ice thickness of 11.3 ML. The symbols refer to 14.5 K (+), 12.4 K (∗), 15.8 K (□), 17.4 K (◇) and 19.3 K (△). The dotted lines indicate the fits to the data.

C_2H_5OH band, the C–O stretching mode, is expected. Since this frequency region is particularly problematic in our detector, the detection upper limit on $N(C_2H_5OH)$ amounts to only 3×10^{15} molecules cm^{-2}, i.e., 3 ML. Another strong band of C_2H_5OH is expected at 3.5 μm. Unfortunately, this feature overlaps with a number of CH_3OH modes. Broad weak features are indeed detected in this range, but due to the complexity of both C_2H_5OH and CH_3OH absorptions and the relatively weak signal this cannot be used to determine whether C_2H_5OH is present. Additionally, it is important to note that no strong features are observed around 2140 cm^{-1}, where both CO and CH_2CO have infrared features. This is perhaps not surprising, because the formation of CO would involve not only the breaking of a C–C bond, but also hydrogen-abstraction, which is not very likely in this hydrogen-rich environment. The formation of ketene, CH_2CO, is even less likely because its formation is strongly endothermic.

The formation of CH_4, H_2CO and CH_3OH is corroborated by the TPD spectra, where 16, 30 and 31 amu mass peaks at 45 K, 100 K and 140 K are found, respectively (see Fig. 8 for CH_4 and CH_3OH). The peaks for 16 amu at higher temperatures are due to O-atoms detected by the mass spectrometer when other molecules dissociate. The desorption temperatures for 16 and 31 amu are similar to those of pure CH_4 and CH_3OH ice confirms their RAIR detection. The TPD spectra and desorption temperatures of 29 amu are consistent with the desorption temperatures for H_2CO found by Watanabe et al. (2004). In addition, a TPD desorption peak is located at ∼160 K for masses 45 and 46 amu (see Fig. 8). This is assigned to C_2H_5OH desorption based on a comparison with the TPD of pure non-bombarded C_2H_5OH ices. In summary, a fraction of CH_3CHO, below the infrared detection limit of the 1050 cm^{-1} band, is converted to C_2H_5OH and a larger fraction forms CH_4, H_2CO and CH_3OH. So even though the conversion of acetaldehyde to ethanol is not complete, it is important to note that a pathway in the proposed hydrogenation scheme by Tielens & Charnley (1997) is experimentally confirmed.

6.2. Reaction rates and production yields

The value for $N(CH_3CHO)$ as derived from the ν_D(umbrella) spectral feature at 1345 cm^{-1} is shown in Fig. 9 as a function of time for different ice thicknesses at 14.5 K. Also shown are the fits to the data. The ν_D(umbrella) mode is chosen for analysis rather than the 1728 cm^{-1} band, because the latter overlaps with the ν_S(C=O) of H_2CO at 1720 cm^{-1}. Clearly, the absolute amount of CH_3CHO that can react increases with ice thickness, whereas A/A_0 decreases. The temperature behavior is more complex and is shown in Fig. 10.

The α_0 and β_0 values derived from the fits as function of the thickness and temperature are shown in Fig. 11. The values for α_0 decrease with increasing thickness, but do not depend on ice temperature within the measured regime. The latter is not surprising as the CH_3CHO ice structure does not change between 15 and 75 K. The value for β_0 is independent of ice thickness, but does depend on ice temperature. It is largest for ice temperatures between 15–16 K, similar to the case of CO (Fuchs et al. 2007). This is expected as the maximum reactivity is mostly determined by the mobility of H-atoms at the surface. At low temperatures H-atoms move more slowly resulting in a lower reaction rate. At higher temperatures the diffusion rate is higher but has to compete with an increased evaporation rate.

For the C_2H_5OH formation, only yields can be calculated from the TPD data because the RAIR feature at 1050 cm^{-1} overlaps with the ν_S(CO) band of CH_3OH. The yields for

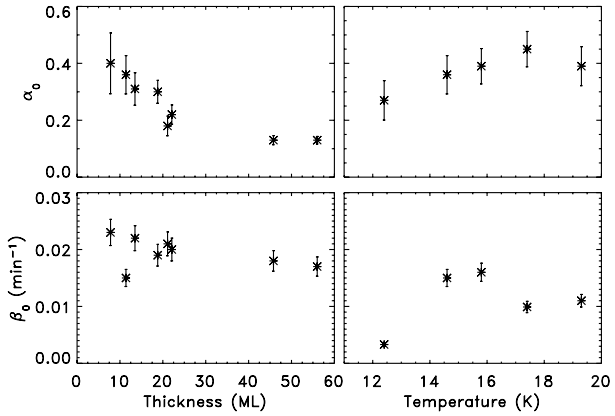

Fig. 11. The α_0 and β_0 dependencies of the CH_3CHO+H reaction on thickness and temperature. The temperature of the ices for the thickness dependence experiments is constant at 14.5 K. The ice thickness is similar for the temperature dependence experiments at 11–12 ML.

CH_4, CH_3OH and C_2H_5OH are given in Table 5. Even when considering that there is a general quantitative uncertainty of ~10%, it is clear that the summed yield of the different products is not 100%. This is most likely due to missing H_2CO yields, because these are not reliably calibrated. Furthermore $Y(CH_4)$ is expected to be equal to $Y(H_2CO+CH_3OH)$, because CH_3OH is formed from H_2CO after CH_3CHO dissociation. However, the CH_3OH yield is significantly higher than CH_4 (see Sect. 6.3). The solid state C_2H_5OH yields are ≤20%.

6.3. Discussion and conclusion

Previously, C_2H_5OH and CH_3CHO were shown to form in interstellar ice analogues by photolysis of C_2H_2:H_2O mixtures (Moore et al. 2001; Wu et al. 2002). Since in such experiments both OH and H fragments are present with excess energy, it is difficult to disentangle potential pure hydrogenation reactions and reactions involving OH radicals. Indeed, Moore & Hudson (2005) explain formation of C_2H_5OH and CH_3CHO by reactions of C_2H_5 and C_2H_3 with OH, respectively. In this paper we focus on the reactions with thermal H-atoms only.

Since H_2CO is known to react with H-atoms to CH_3OH (Watanabe et al. 2004; Hidaka et al. 2004) it is thus likely that the next more complex aldehyde, acetaldehyde (CH_3CHO), will form ethanol (C_2H_5OH). In Fig. 12 the relative heats of formation at 0 K are shown (Wiberg et al. 1991; Cox et al. 1989; Gurvich et al. 1989; Frenkel et al. 1994; Matus et al. 2007). The exothermicity of CH_3CHOH formation is higher than that of CH_3CH_2O, but which of the species is more likely formed depends on the reaction barriers. Subsequent formation of C_2H_5OH is likely fast, because reactions of radicals with H-atoms commonly have no activation barriers. As described in Sect. 6.2 only a fraction of CH_3CHO is converted to C_2H_5OH, and a larger fraction leads to CH_4, H_2CO, and CH_3OH formation. For hydrogenation of CH_3CHO a C=O bond is converted to a C–O bond instead of breaking a C–C bond. Since the C=O bond is intrinsically stronger it is likely that the entrance channel to hydrogenation is higher in energy compared to dissociation.

Thus H-atoms can break the C–C bond as well as the C=O bond to form CH_4, H_2CO and CH_3OH or C_2H_5OH in ices as prepared here. As shown in Fig. 12 the formation of CH_4+HCO is more exothermic than that for CH_3+H_2CO. Furthermore, the energy released in this step is higher than the binding energy of CH_4 to the surface, which is ~700 K (0.06 eV). This likely explains why the $Y(CH_4)$ is lower than $Y(CH_3OH+H_2CO)$, because the formation energy is sufficient for CH_4 desorption. The energy released during the formation of H_2CO, CH_3OH and C_2H_5OH is even higher and may also cause a fraction of the molecules to desorb.

7. Astrophysical implications

Our experiments show that CO_2 reaction rates with H-atoms are very low, making it an implausible route for HCOOH formation. A number of other HCOOH formation routes are possible (see e.g., Milligan & Jacox 1971; Hudson & Moore 1999; Keane 2001), from either HCO+OH → HCOOH or HCO+O → HCOO+H → HCOOH. In addition, experiments suggest that under specific catalytic conditions CO_2 can react to form HCOOH (Ogo et al. 2006) but this requires catalytic surface sites, i.e., CO_2 directly attached to a silicate or metallic grain site. Such a situation is less likely in dense interstellar clouds where thick ice layers have already formed and cover any potential catalytic sites. In conclusion, under astrophysically relevant conditions solid CO_2 in bulk ice is a very stable molecule that is not likely to react with H-atoms.

Similar to CO_2, reaction rates of HCOOH with H-atoms are below the detection limit in our experiment. Formation of the so far undetected interstellar species $CH_2(OH)_2$ in this way thus seems unlikely. Unless other formation mechanisms are found an observational search for this species based upon solid state astrochemical arguments is not warranted. We conclude that CO_2, HCOOH and $CH_2(OH)_2$ do not appear to be related through successive hydrogenation in interstellar ice analogues under the conditions as used in the present study.

In contrast to CO_2 and HCOOH, CO does react with H-atoms. The reaction rates of CO in CO:CO_2 mixtures are very similar to those found by Fuchs et al. (2007) for pure CO ices. CO hydrogenation in interstellar ices will thus not be strongly affected by the presence of CO_2 in the ice. It is likely that the reaction rate is the same for H+CO independent of the CO concentration and that of other species in apolar interstellar ices.

Reactions of CH_3CHO in interstellar ices proceed at similar rates compared to CO hydrogenation. A maximum of 20% will be converted to ethanol, C_2H_5OH, while another major reaction channel leads to CH_4, H_2CO and CH_3OH. The precise abundance of CH_3CHO in interstellar ice is not yet well determined. However, abundances of 1–5% are quoted in the literature (Schutte et al. 1997, 1999; Gibb et al. 2004; Boogert et al. 2004). These values can be used to derive an upper limit on the C_2H_5OH abundance that could thus be formed. As an example we compare the abundances for the high mass source W 33A, where CH_3CHO has a solid state abundance of 9.8×10^{-6} and CH_3OH of $1.4–1.7 \times 10^{-5}$ both with respect to H_2. If we assume that all solid CH_3CHO is present in the surface layer and the C_2H_5OH yield is ~20%, an abundance of C_2H_5OH of at most 2.0×10^{-6} with respect to H_2 can be formed. This leads to an upper limit on the C_2H_5OH/CH_3OH ratio of 0.14. In reality this value will be lower as part of the CH_3CHO ice may be shielded from incoming H-atoms and other destruction reactions will likely be competing with hydrogenation reactions. The limit of 0.14 is clearly higher than the observationally derived C_2H_5OH/CH_3OH abundance ratio in the gas phase of 0.025 ± 0.013 (Bisschop et al. 2007b). Formation of C_2H_5OH from solid state hydrogenation of CH_3CHO is thus sufficient to explain the observed abundances of C_2H_5OH.

Table 5. Values for α_0, β_0, the reaction rate k_0 for CH_3CHO, and production yields, Y(X) upon H-atom bombardment. The uncertainties for α_0 and β_0 amount to 10–20%, for k_0 are a factor 2 and Y 20%.

Ice temperature (K)	Ice thickness (ML)	α_0	β_0 (min^{-1})	k_0 ($cm^2\ s^{-1}$)	$Y(C_2H_5OH)$ (%)	$Y(CH_4)$ (%)	$Y(CH_3OH)$ (%)
14.5	7.8	0.40	2.3(−2)	2.8(−15)	15	21	
14.5	11.4	0.36	1.5(−3)	1.8(−16)	10	19	
14.6	13.5	0.31	2.2(−2)	2.6(−15)	14	22	48
14.5	18.8	0.30	1.9(−2)	2.3(−15)	13	18	
14.5	21.2	0.18	2.1(−2)	2.5(−15)	17	24	
14.6	22.1	0.22	2.0(−2)	2.4(−15)	20	23	39
14.6	45.8	0.13	1.8(−2)	2.2(−15)	20	21	38
14.6	56.0	0.13	1.7(−2)	2.0(−15)	20	17	35
15.8	11.6	0.39	1.6(−3)	1.9(−16)	21	22	33
17.4	11.3	0.45	9.9(−3)	1.2(−15)	16	19	
19.3	11.2	0.39	1.1(−2)	1.3(−15)	14	13	15

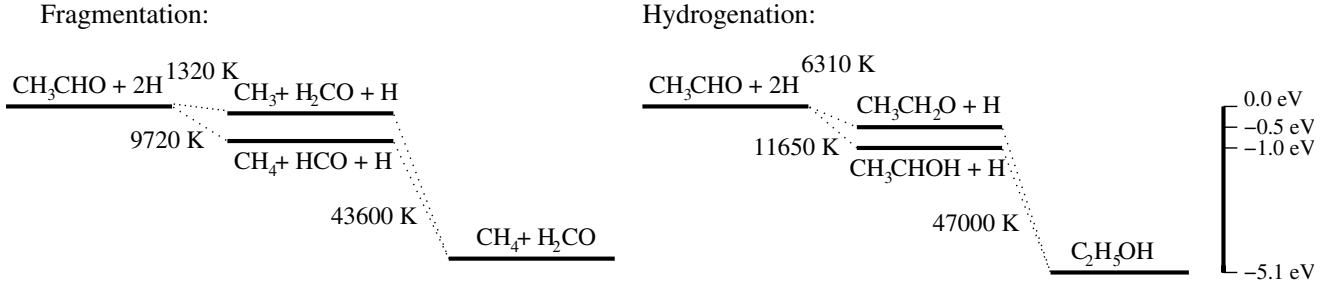

Fig. 12. Potential energy scheme for CH_3CHO fractionation and hydrogenation. The relative energies are based on the heats of formations at 0 K. An approximate energy scale in electronvolts is given on the right. The heats of formation are derived from Wiberg et al. (1991) for CH_3CHO, Cox et al. (1989) for H, Gurvich et al. (1989) for CH_3, H_2CO, CH_4 and HCO, Frenkel et al. (1994) for C_2H_5OH and Matus et al. (2007) for the CH_3CHOH and CH_3CH_2O radicals.

8. Summary and conclusions

Hydrogenation reactions of CO_2, HCOOH and CH_3CHO interstellar ice analogues have been studied under ultra-high vacuum conditions. RAIRS and TPD have been used to analyze the results. From these experiments reaction rates and upper limits on destruction and formation rates of the above mentioned species are calculated. The main conclusions derived from this work are:

- CO_2 and HCOOH do not react with H-atoms at a detectable level. Only minor fractions of the species desorb due to the bombardment. Solid state formation of HCOOH from CO_2 and $CH_2(OH)_2$ from HCOOH are likely inefficient in interstellar ices.
- Hydrogenation of CO to H_2CO and CH_3OH from CO mixed with CO_2 has similar reaction rates compared to pure CO ices. The presence of CO_2 in interstellar ices with CO therefore does not affect the formation of H_2CO and CH_3OH.
- Hydrogenation of CH_3CHO leads for ∼20% to C_2H_5OH, showing for the first time that a thermal hydrogenation reaction can be responsible for the C_2H_5OH abundances detected in dense interstellar clouds. Other reaction products are H_2CO, CH_3OH (15–50%) and CH_4 (∼10%). Due to the energy released a fraction of the produced species may evaporate into the gas phase upon formation.

Acknowledgements. Funding was provided by NOVA, the Netherlands Research School for Astronomy and by a Spinoza grant from the Netherlands Organization for Scientific Research, NWO. We thank Sergio Ioppolo for help with the experiments, Herma Cuppen for the theoretical simulations of hydrogen flux in our experiment, Karin Öberg for stimulating discussions and an anonymous referee for constructive comments on the paper.

References

Allamandola, L. J., Sandford, S. A., & Valero, G. J. 1988, Icarus, 76, 225
Andersson, S., Al-Halabi, A., Kroes, G.-J., & van Dishoeck, E. F. 2006, J. Chem. Phys., 124, 4715
Benitez, J. J., Carrizosa, J., & Odriozola, J. A. 1993, Appl. Surf. Sci., 68, 565
Bennett, C. J., Jamieson, C. S., Osamura, Y., & Kaiser, R. I. 2005, ApJ, 624, 1097
Bisschop, S. E., Fuchs, G. W., Boogert, A. C. A., van Dishoeck, E. F., & Linnartz, H. 2007a, A&A, 470, 749
Bisschop, S. E., Jørgensen, J. K., van Dishoeck, E. F., & de Wachter, E. B. M. 2007b, A&A, 465, 913
Blake, G. A., Sutton, E. C., Masson, C. R., & Phillips, T. G. 1987, ApJ, 315, 621
Boogert, A. C. A., Pontoppidan, K. M., Lahuis, F., et al. 2004, ApJS, 154, 359
Bouwman, J., Ludwig, W., Awad, Z., et al. 2007, A&A, in press
Cox, J. D., Wagman, D. D., & Medvedev, V. A. 1989, CODATA Key Values for Thermodynamics (Hemisphere Publishing Corp.)
Cyriac, J., & Pradeep, T. 2005, Chem. Phys. Lett., 402, 116
Ehrenfreund, P., Kerkhof, O., Schutte, W. A., et al. 1999, A&A, 350, 240
Ewing, G. E., Thompson, W. E., & Pimentel 1960, J. Chem. Phys., 32, 927
Frenkel, M., Marsh, K. N., Wilhoit, R. C., Kabo, G. J., & Roganov, G. N. 1994, Thermodynamics of Organic Compounds in the Gas State (Texas, USA: Thermodynamics Research Center)
Fuchs, G. W., Ioppolo, S., Bisschop, S. E., Van Dishoeck, E. F., & Linnartz, H. 2007, A&A, submitted
Gerakines, P. A., Moore, M. H., & Hudson, R. L. 2000, A&A, 357, 793

Gibb, E. L., Whittet, D. C. B., Boogert, A. C. A., & Tielens, A. G. G. M. 2004, ApJS, 151, 35
Gurvich, L. V., Veyts, I. V., & Alcock, C. B. 1989, Thermodynamic Properties of Individual Substances, 4th edn. (New York: Hemisphere Pub. Co.)
Hidaka, H., Watanabe, N., Shiraki, T., Nagaoka, A., & Kouchi, A. 2004, ApJ, 614, 1124
Hiraoka, K., Ohashi, N., Kihara, Y., et al. 1994, Chem. Phys. Lett., 229, 408
Hiraoka, K., Sato, T., Sato, S., et al. 2002, ApJ, 577, 265
Hudson, R. L., & Moore, M. H. 1999, Icarus, 140, 451
Hwang, D. Y., & Mebel, A. M. 2004, J. Phys. Chem. A, 108, 10245
Ikeda, M., Ohishi, M., Nummelin, A., et al. 2001, ApJ, 560, 792
Keane, J. V. 2001, Ph.D. Thesis, Rijks Universiteit Groningen
Keane, J. V., Tielens, A. G. G. M., Boogert, A. C. A., Schutte, W. A., & Whittet, D. C. B. 2001, A&A, 376, 254
Lakin, M. J., Troya, D., Schatz, G. C., & Harding, L. B. 2003, J. Chem. Phys., 119, 5848
Lugez, C., Schriver, A., Levant, R., & Schriver-Mazzuoli, L. 1994, Chem. Phys., 181, 129
Matus, M. H., Nguyen, M. T., & Dixon, D. H. 2007, J. Phys. Chem. A, 111, 113
Milligan, D. E., & Jacox, M. E. 1964, J. Chem. Phys., 41, 3032
Milligan, D. E., & Jacox, M. E. 1971, J. Chem. Phys., 54, 927
Moore, M. H., & Hudson, R. L. 1998, Icarus, 135, 518
Moore, M. H., & Hudson, R. L. 2003, Icarus, 161, 486
Moore, M. H., & Hudson, R. L. 2005, in Astrochemistry: Recent Successes and Current Challenges, ed. D. C. Lis, G. A. Blake, & E. Herbst, IAU Symp., 231, 247
Moore, M. H., Hudson, R. L., & Gerakines, P. A. 2001, Spectrochim. Acta A, 57, 843
Öberg, K. I., Fraser, H. J., Boogert, A. C. A., et al. 2007, A&A, 462, 1187
Ogo, S., Kabe, R. H. H., Harada, R., & Fukuzumi, S. 2006, Dalton T., 39, 4657
Ruscic, B., Wagner, A. F., Harding, L. B., et al. 2002, J. Chem. Phys. A, 106, 2727
Schutte, W. A., Boogert, A. C. A., Tielens, A. G. G. M., et al. 1999, A&A, 343, 966
Schutte, W. A., Greenberg, J. M., van Dishoeck, E. F., et al. 1997, Ap&SS, 255, 61
Tielens, A. G. G. M., & Charnley, S. B. 1997, Origins Life Evol. B., 27, 23
Tschersich, K. G. 2000, J. Appl. Phys., 87, 2565
Tschersich, K. G., & von Bonin, V. 1998, J. Appl. Phys., 84, 4065
Van Ijzendoorn, L. J., Allamandola, L. J., Baas, F., & Greenberg, J. M. 1983, J. Chem. Phys., 78, 7019
Watanabe, N., Nagaoka, A., Shiraki, T., & Kouchi, A. 2004, ApJ, 616, 638
Wiberg, K. B., Crocker, L. S., & Morgan, K. M. 1991, J. Am. Chem. Soc, 113, 3447
Wu, C. Y. R., Judge, D. L., Cheng, B.-M., et al. 2002, Icarus, 156, 456